Available online at www.sciencedirect.com
ScienceDirect
Journal of Catalysis 246 (2007) 118–126
JOURNAL OF CATALYSIS
www.elsevier.com/locate/jcat

In situ IR study of adsorbed species and photogenerated electrons during photocatalytic oxidation of ethanol on TiO_2

Zhiqiang Yu, Steven S.C. Chuang *

Department of Chemical and Biomolecular Engineering, University of Akron, Akron, OH 44325-3906, USA

Received 11 September 2006; revised 17 November 2006; accepted 21 November 2006

Available online 26 December 2006

Abstract

The reaction pathways for the photocatalytic oxidation of ethanol on the TiO_2 surface at 30 °C were studied by in situ infrared (IR) spectroscopy. The coverage of ethanol and water was found to play a key role in how the reaction is initiated. The low ethanol coverage on the H_2O_{ad}-containing TiO_2 surface produced adsorbed formate ($HCOO^-_{ad}$) as a primary intermediate; the high ethanol coverage on the H_2O_{ad}-deficient TiO_2 surface produced adsorbed acetate ($CH_3COO^-_{ad}$) as a major intermediate during the initial period (i.e., 2 min) of the photocatalytic oxidation. The adsorbed species and reaction products observed during in situ IR studies suggest the low-coverage ethanol reaction is initiated by •OH, whereas the high-coverage ethanol reaction is initiated by hole. The hole-initiating ethanol oxidation on the H_2O_{ad}-deficient TiO_2 surface produced adsorbed acetic acid (CH_3COOH_{ad})/$CH_3COO^-_{ad}$, and built up photogenerated electrons, giving a parallel increase in the IR intensity of $CH_3COO^-_{ad}$ and the IR background at 2000 cm^{-1} (i.e., a measure of photogenerated electrons). As the high-coverage ethanol reaction proceeded toward producing CO_2/H_2O, adsorbed H_2O accumulated and the coverage of $CH_3CH_2OH_{ad}/CH_3CH_2O_{ad}$ decreased on the TiO_2 surface, shifting the reaction from hole-initiating to •OH-initiating.

Keywords: Photocatalytic oxidation; Ethanol; Adsorbed species; Reaction mechanism; In situ infrared spectroscopy; Photogenerated electrons

1. Introduction

Photocatalytic reactions are characterized by the transfer of light-induced charge carriers (i.e., photogenerated electron and hole pairs) to the electron donors and acceptors adsorbed on the semiconductor catalyst surface [1–6]. The electron and hole pairs produced in the bulk of the semiconductor catalyst may undergo recombination and trapping before reaching the catalyst surface to transfer their charges to the electron donors and acceptors. The rates of charge recombination, trapping, and transfer determine the quantum efficiency of the photocatalytic reaction.

A number of spectroscopic studies have revealed the dynamic behavior of electron/hole pairs [1,3,4,7]. The electron/hole generation process has been shown to occur on the TiO_2 surface at a time scale of femtoseconds; the interfacial charge transfer from the TiO_2 surface to adsorbed species occurs in the range of 10–100 ns. In contrast, the time scale for the electron/hole recombination process can vary from 100 ps to days, depending on the surface state of the TiO_2 semiconductor [7–11].

A useful technique for studying electron/hole recombination and trapping is infrared (IR) spectroscopy, which shows that the photogenerated electrons give a structureless IR absorption spectrum from 3000 to 900 cm^{-1} [7–11]. Addition of O_2 onto the TiO_2 surface causes a decay of the structureless IR absorbance, with a half-life ($t_{1/2}$, the time required for the intensity of an IR band to drop to half of its initial value) of about 100 s at −133 °C [11]. Half-life has also been shown in the range of 10 s–180 min for the IR bands of a number of intermediate species observed during the photocatalytic oxidation of alcohols and acetone on the TiO_2 surface [12–15]. The long half-life of photogenerated electrons and photocatalytic oxidation intermediates on the TiO_2 surface allows simultane-

* Corresponding author. Fax: +1 330 972 5856.
E-mail address: schuang@uakron.edu (S.S.C. Chuang).

0021-9517/$ – see front matter
doi:10.1016/j.jcat.2006.11.022

ous measurements of changes in IR spectra of photogenerated electrons and adsorbed species.

The objective of the present study is to determine the dynamic behavior of IR-observable species and their relations to photogenerated electrons during the photocatalytic oxidation (PCO) of ethanol on the TiO_2 surface. In the present study, the diffuse reflectance infrared Fourier transform spectroscopy (DRIFTS) spectra of the photocatalytic oxidation of the high and low-coverage ethanol on the TiO_2 surface were taken from 1050 to 4000 cm^{-1}, covering the spectra of key reaction intermediates and the photogenerated electrons. The reaction pathway for the photocatalytic oxidation of ethanol was elucidated from the evolution of IR intensities of ethanol, reaction intermediates, CO_2, adsorbed H_2O (H_2O_{ad}), and photogenerated electrons.

2. Experimental

The apparatus for the in situ IR photocatalytic oxidation studies consisted of three parts: (i) a DRIFTS cell from Harrick Scientific (HVC-DRP), (ii) a Xe 350 W mercury lamp (Oriel 6286) with a light condenser (Oriel 77800), and (iii) a flow manifold to allow admission of oxygen and ethanol vapor into the DRIFTS cell. A 15-mg sample of TiO_2 catalyst (Degussa P25, ~50 m^2/g, approximately 70% anatase and 30% rutile) was placed on top of 80 mg of inert CaF_2 powder (325 mesh, Alfa Aesar) in a sample holder 6.4 mm in diameter, as shown in Fig. 1. The sample holder was enclosed by a three-windowed dome. Two of these windows (ZnSe) were IR transparent, whereas the third one (CaF_2) permitted UV illumination with the intensity of 25 mW/cm^2. The DRIFTS cell resided in a FTIR (DigiLab FTS 4000) bench.

Ethanol photocatalytic oxidation was carried out on the TiO_2 surface with ultra-high purity O_2 (Praxair, 99.999%) in the DRIFTS cell at 30 °C and 1 atm for 120 min. The amount of adsorbed ethanol on the TiO_2 catalyst was controlled by controlling the duration of flowing O_2 with saturated ethanol (10.3 mol% of ethanol in O_2) at a rate of 15 cm^3/min through the DRIFTS cell.

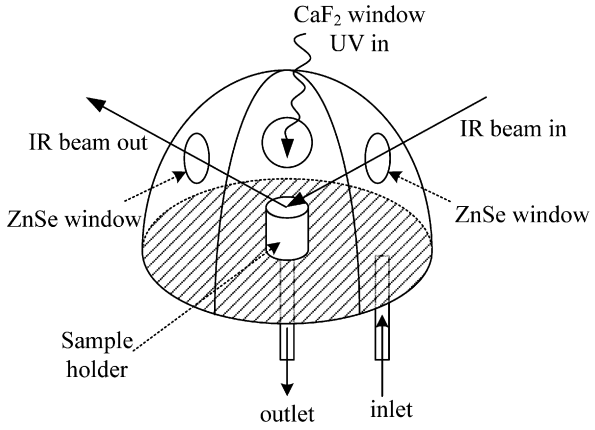

Fig. 1. DRIFTS cell for photocatalytic oxidation of ethanol.

3. Results

Fig. 2 shows the IR spectra of ethanol adsorption on the TiO_2 surface at 30 °C. Exposure of TiO_2 to flowing O_2/ethanol for 2 s (Fig. 2a) and for 10 min (Fig. 2b), followed by O_2 purging for 20 min (i.e., flowing O_2 to remove gaseous ethanol), produced 341 and 713 μmol of adsorbed ethanol per gram of TiO_2 catalyst, respectively. For convenience, the former is designated as a low-coverage ethanol, and the latter as high-coverage ethanol. The amount of adsorbed ethanol was determined by the carbon balance between adsorbed ethanol and the CO_2 product with their IR intensities and extinction coefficients.

Table 1 summarizes the IR band assignments for adsorbed ethanol and species appearing during the photocatalytic reactions on the TiO_2 surface [12–18]. The adsorption of ethanol on the TiO_2 surface at 30 °C formed both molecularly adsorbed and dissociatively adsorbed ethanol (adsorbed ethoxy). Although the molecularly adsorbed ethanol ($CH_3CH_2OH_{ad}$) and adsorbed ethoxy ($CH_3CH_2O_{ad}$) exhibited similar bands of C–H stretching vibrations at 2971 and 2931 cm^{-1}, as well as a C–O stretching vibration at 1052 cm^{-1}, their behaviors differed under O_2 flow. The rapid decrease in intensity of 2971, 2931, and 1052 cm^{-1} in high-coverage ethanol, shown in Fig. 2b, resulted from partial removal of $CH_3CH_2OH_{ad}$ from the TiO_2 surface in flowing O_2. After 20 min of O_2 flow, the species remained on the surface exhibited the bands at 2971, 2931, 1380, and 1113 cm^{-1} with a similar intensity. Most of these species could be attributed to $CH_3CH_2O_{ad}$ on the TiO_2 surface. This is in contrast to gaseous and liquid ethanol, which typically give a high IR intensity ratio at the 2971/2931 cm^{-1} and 1052/1113 cm^{-1} bands [16]. Thus, the IR intensity ratio of these bands could reflect the relative concentration of $CH_3CH_2OH_{ad}/CH_3CH_2O_{ad}$ on the TiO_2 surface.

Comparing the IR intensities of low- and high-coverage ethanol in Fig. 2 shows that the IR intensity of high-coverage ethanol was about twice that of low-coverage ethanol, corresponding to their molar ratios (i.e., 713 vs 341 μmol). The high-coverage ethanol displaced significantly more H_2O_{ad} from the TiO_2 surface than the low-coverage ethanol. Displacement of H_2O_{ad} produced a negative isolated OH band at 3690 cm^{-1} and two strong negative H_2O_{ad} bands at 3550 and 1635 cm^{-1}. Although we were not able to determine the amount of H_2O_{ad}, the negative intensity of the H_2O_{ad} band resulting from high-coverage ethanol on the TiO_2 surface is equivalent to that from a TiO_2 surface dehydrated at 400 °C. Thus, it can be concluded that the low-coverage ethanol is adsorbed on the H_2O_{ad}-containing surface, and the high-coverage ethanol is adsorbed on the H_2O_{ad}-deficient surface.

Figs. 3 and 4 show the IR spectra of the low-coverage ethanol reaction on the H_2O_{ad}-containing TiO_2 surface. The IR spectra in Fig. 3a show that the intensities of the C–H stretching at 2971, 2931, and 2872 cm^{-1}, the OH stretching of $CH_3CH_2OH_{ad}$ at 1274 cm^{-1}, and the C–O monodentate stretching of $CH_3CH_2O_{ad}$ at 1113 cm^{-1} decreased rapidly from 0 to 2 min upon UV illumination. Because of the overlap of the bands of $CH_3CH_2OH_{ad}$ and $CH_3CH_2O_{ad}$ with the bands of the intermediate species produced during the reaction, the in-

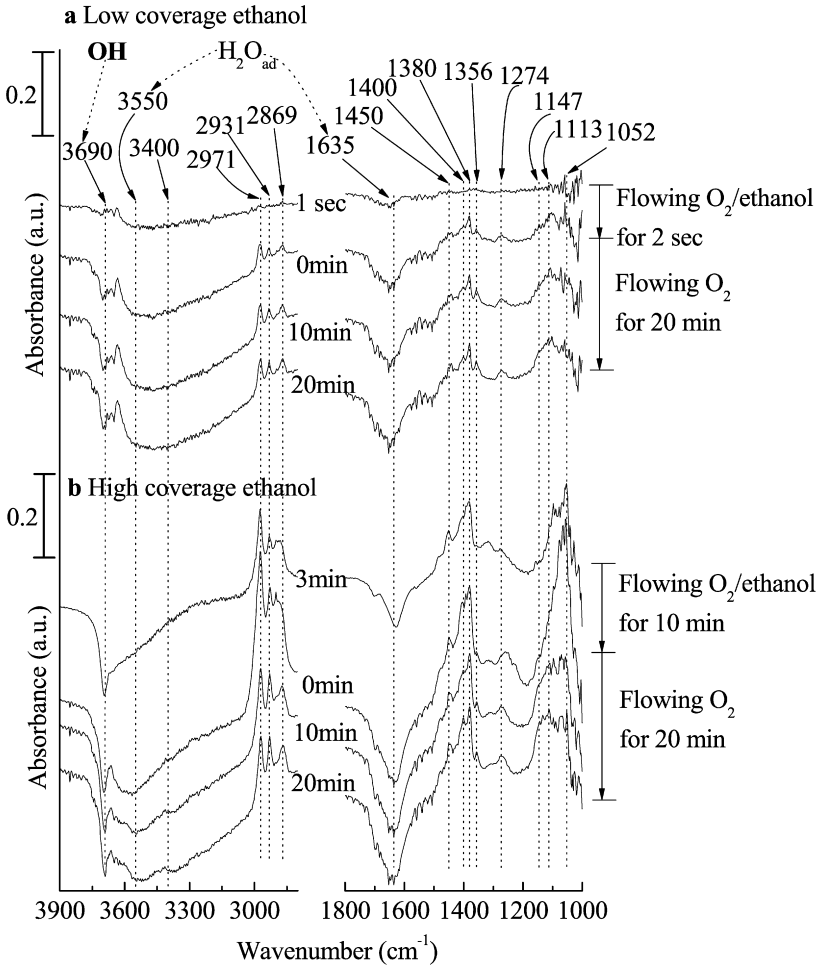

Fig. 2. IR spectra of ethanol absorption on TiO_2 at 30 °C; (a) low coverage ethanol, (b) high coverage ethanol.

Table 1
Band assignments and their vibration modes

Species	Bands (cm^{-1}) and modes
$C_2H_5OH_{ad}$	ν(HO···H)/3400; $\nu_{as}(CH_3)$/2971; $\nu_{as}(CH_2)$/2931; $\nu_s(CH_3)$/2901; $\delta_s(CH_3)$/1400; δ(OH)/1274; ν(C–O)/1052;
$C_2H_5O_{ad}$	$\nu_{as}(CH_3)$/2971; $\nu_{as}(CH_2)$/2931; $\nu_s(CH_3)$/2872, 2869; $\delta_{as}(CH_2)$/1450; $\delta_s(CH_2)$/1380, 1379; CH_2 wagging/1356; ν(C–O) monodentate/1147, 1113; ν(C–O) bidentate/1052;
CH_3CHO_{ad}	ν(C=O)/1723, 1721, 1718;
CH_3COOH_{ad}	ν(C=O)/1684;
$CH_3COO^-_{ad}$	ν_{as}(COO)/1542, 1537; $\delta_{as}(CH_3)$/1469; ν_s(COO)/1446, 1443, 1438, 1421; $\delta_s(CH_3)$/1340;
$HCHO_{ad}$	ν(C=O)/1619;
$HCOOH_{ad}$	ν(C=O)/1691;
$HCOO^-_{ad}$	ν(CH)/2846; ν_{as}(COO)/1581, 1573; δ(CH)/1416; ν_s(COO)/1350;
Isolated –OH	ν(OH)/3692, 3690, 3634;
H_2O_{ad}	ν(HO···H)/3550; δ(OH)/1650, 1635;
CO_2	ν_{as}(C=O)/2362;

tensity variations for those IR bands in the 1300–1750 cm^{-1} region must be revealed through the difference spectra obtained by subtracting the spectrum at 0 min (i.e., before the reaction) from the subsequent spectra. For example, the first difference spectrum (0.25–0 min) in Fig. 3b was obtained by subtracting the spectrum at 0 min from the spectrum at 0.25 min in Fig. 3a. The difference spectrum (0.25–0 min) in Fig. 3b shows the rapid formation of adsorbed formic acid ($HCOOH_{ad}$) at 1691 cm^{-1}; adsorbed formaldehyde ($HCHO_{ad}$) at 1619 cm^{-1}; adsorbed formate ($HCOO^-_{ad}$) at 1581, 1416, 1369, and 1350 cm^{-1}; adsorbed acetate ($CH_3COO^-_{ad}$) at 1542 and 1446 cm^{-1}; and CO_2 at 2362 cm^{-1} upon UV illumination. Subsequent difference spectra show that the IR intensities of $HCOOH_{ad}$ and $HCHO_{ad}$ gradually decreased after reaching a maximum, but those of $CH_3COO^-_{ad}$, $HCOO^-_{ad}$, and CO_2 increased at a significant rate during the first 2 min of the low-coverage ethanol reaction. Adsorbed acetaldehyde (CH_3CHO_{ad}) exhibited an increasing intensity at 1721 cm^{-1} in Fig. 3b and became a prominent band at 1718 cm^{-1} after 20 min of the reaction in Fig. 4.

Fig. 4 shows the IR spectra and difference spectra of CO_2, H_2O_{ad}, and adsorbed species during the entire 120 min of the reaction. The absence of appreciable C–H stretching bands at 2971, 2931, and 2872 cm^{-1} and the C–O stretching band at 1113 cm^{-1} after 10 min of the reaction, shown in Fig. 4a, suggests that both $CH_3CH_2OH_{ad}$ and $CH_3CH_2O_{ad}$ were nearly depleted. Although $HCOO^-_{ad}$, $HCOOH_{ad}$, $CH_3COO^-_{ad}$, CH_3COOH_{ad}, and CH_3CHO_{ad} produced from $CH_3CH_2OH_{ad}$/$CH_3CH_2O_{ad}$ have C–H bonds, these species give a very low C–H stretching intensity [19,20] and their formation cannot compensate for the loss of C–H stretching intensity from break-

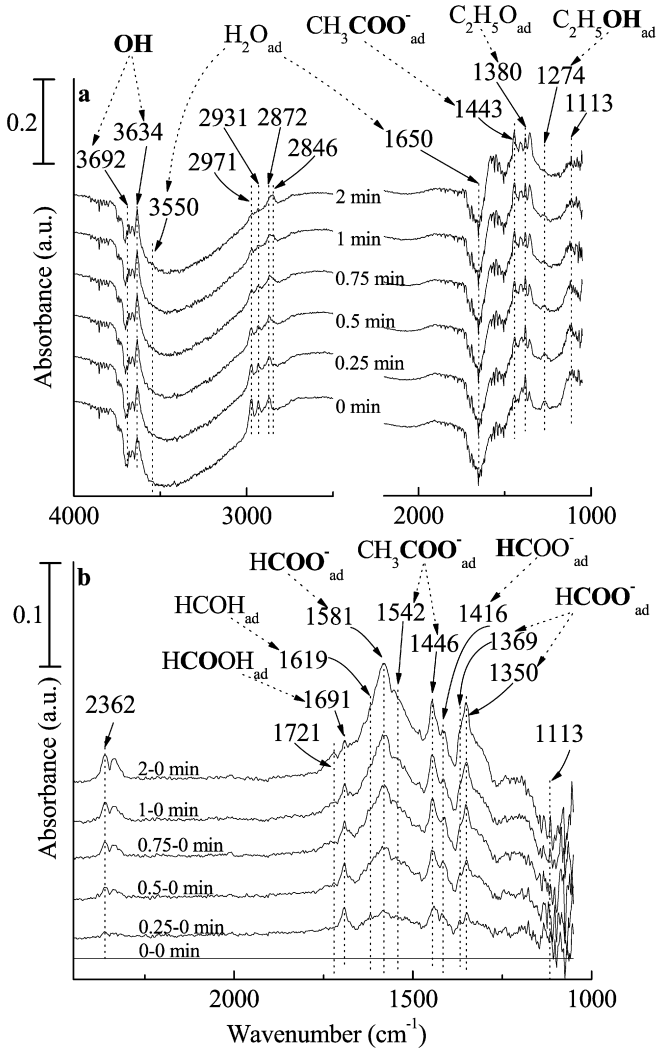

Fig. 3. (a) IR spectra and (b) difference spectra during the first 2 min of photocatalytic oxidation of low coverage ethanol.

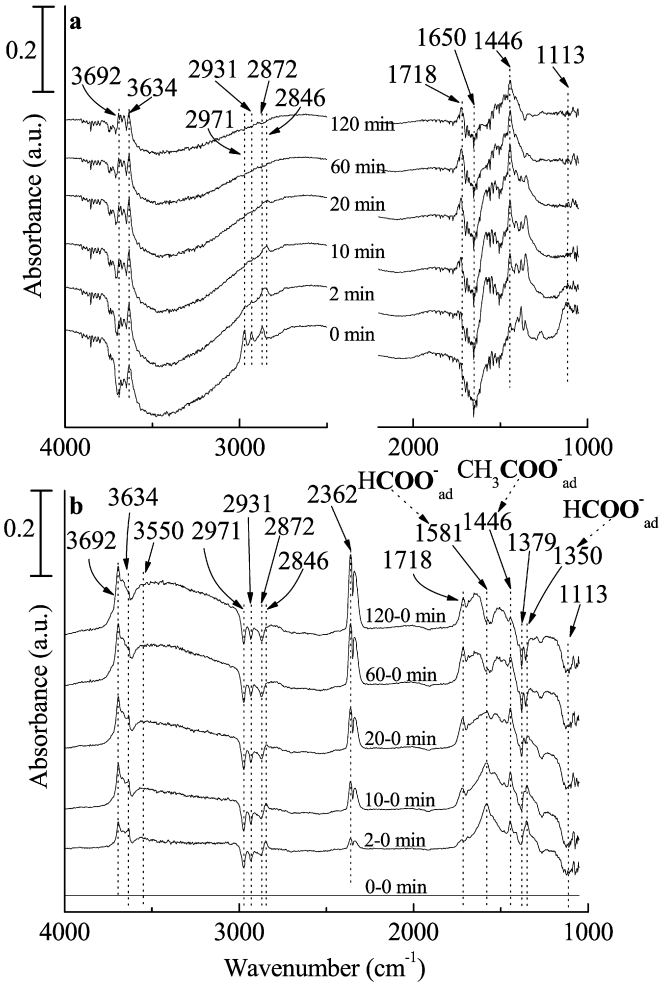

Fig. 4. (a) IR spectra and (b) difference spectra during 120 min of photocatalytic oxidation of low coverage ethanol.

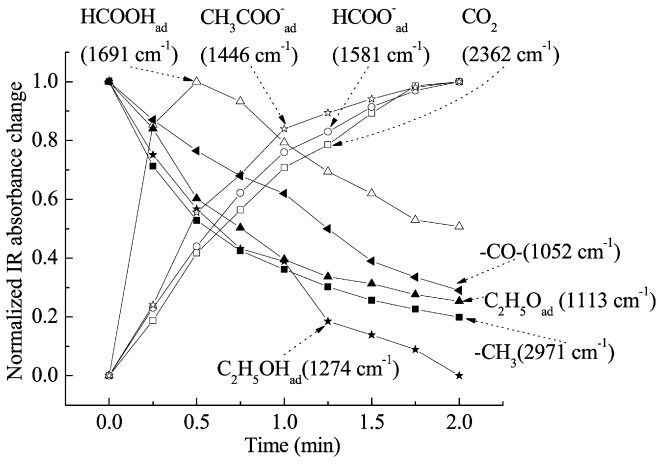

Fig. 5. Variation of the normalized IR intensity of adsorbed species and CO_2 as a function of time during the first 2 min of the photocatalytic oxidation of low coverage ethanol. Normalized intensity $= I(t)/I_{max}$, where $I(t)$: intensity of a species at time of t; I_{max}: the maximum intensity of a species during the first 2 min.

ing of the C–H bonds in $CH_3CH_2OH_{ad}/CH_3CH_2O_{ad}$. The variation of the IR intensity of $HCOO^-_{ad}/CH_3COO^-_{ad}$ can be discerned from the difference spectra shown in Fig. 4b. These IR spectra show $HCOO^-_{ad}$ at 1581 cm^{-1} grew to a maximum IR intensity at about 2 min and $CH_3COO^-_{ad}$ at 1446 cm^{-1} reached a maximum at 20 min, while the IR intensity of H_2O_{ad} and CO_2 increased gradually during the entire 120 min of the reaction.

The normalized intensities of IR observable species with time in Figs. 5 and 6 reveal that the time (t_{max}) when the species reach their maximum IR intensities increased in the order: $HCOOH_{ad} < HCOO^-_{ad} < CH_3COO^-_{ad} < CH_3CHO_{ad}$, indicating that the formation of $HCOOH_{ad}$ led that of $HCOO^-_{ad}$ and the formation of $HCOO^-_{ad}$ led that of $CH_3COO^-_{ad}$. In addition, the results in Fig. 3b show that the formation of $HCHO_{ad}$ led that of $HCOOH_{ad}$. If the photocatalytic oxidation of ethanol to CO_2/H_2O follows a series (i.e., A → B → C → ⋯ → G) reaction pathway, then the reaction would proceed through $CH_3CH_2OH_{ad}/CH_3CH_2O_{ad}$ → $HCHO_{ad}$ → $HCOOH_{ad}$ → $HCOO^-_{ad}$ → $CH_3COO^-_{ad}$ → CH_3CHO_{ad} → CO_2/H_2O according to the t_{max} of each IR-observable species [21]. However, the conversion of a C_1-oxygenated species (i.e., $HCOOH_{ad}/HCOO^-_{ad}$) to a C_2-oxygenated species (i.e., $CH_3COO^-_{ad}/CH_3CHO_{ad}$) is not possible in a photooxidation

pathway. It is likely that both C_1-oxygenated and C_2-oxygenated species were produced from parallel pathways in the photocatalytic oxidation of low-coverage ethanol. $HCOOH_{ad}$/$HCOO^-_{ad}$ could be directly produced from $CH_3CH_2OH_{ad}$/$CH_3CH_2O_{ad}$ without going through adsorbed acetic acid (CH_3COOH_{ad})/$CH_3COO^-_{ad}$ as intermediate steps. This is in contrast to the proposed pathway from the analysis of gaseous products of a PCO study: $CH_3CH_2OH \rightarrow CH_3CHO \rightarrow CH_3COOH \rightarrow HCHO \rightarrow HCOOH \rightarrow CO_2$ [22]. However, careful examination of the product profiles of this PCO study [22] shows that CH_3COOH and HCHO evolved at the same initial time, suggesting that HCHO can be formed from ethanol without involving CH_3COOH as an intermediate species. Results of previous IR studies suggest that $CH_3CH_2O_{ad}$ led to the formation of $HCOO^-_{ad}$, $CH_3COO^-_{ad}$, and H_2O_{ad}, whereas $CH_3CH_2OH_{ad}$ resulted in the production of CH_3CHO_{ad}/$CH_3COO^-_{ad}$ [12,13]. Results of PCO coupled with temperature-programmed desorption (PCO/TPD) studies suggest that weakly bound ethanol tended to form CH_3CHO_{ad}, whereas strongly bound ethanol produced CO_2 via

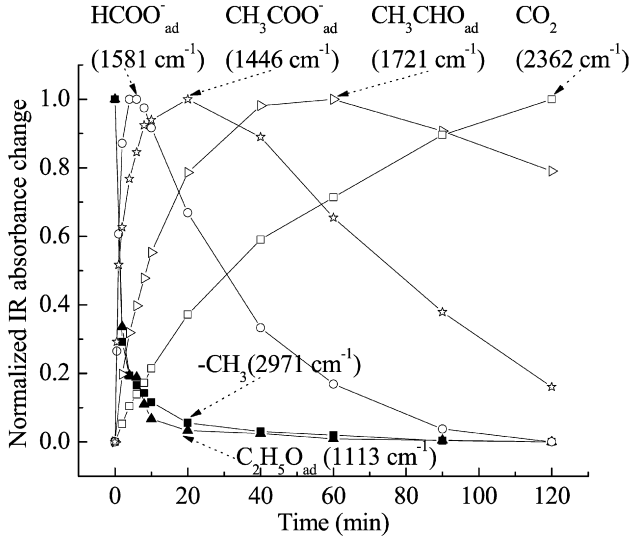

Fig. 6. Variation of the normalized IR intensity of adsorbed species and CO_2 as a function of time during 120 min of the photocatalytic oxidation of low coverage ethanol. Normalized intensity $= I(t)/I_{max}$, where $I(t)$: intensity of a species at time of t; I_{max}: the maximum intensity of a species during the 120 min.

two pathways: (i) $CH_3CHO_{ad} \rightarrow CH_3COOH_{ad} \rightarrow HCHO_{ad} \rightarrow HCOOH_{ad}$ and (ii) $CH_3CHO_{ad} \rightarrow HCHO_{ad}/HCOOH_{ad}$ [23,24].

Considering these suggested pathways [12,13,22–25] along with our direct IR observations of the evolution of adsorbed species produced during the low-coverage ethanol reaction, a parallel/series pathway for the conversion of ethanol to CO_2/H_2O_{ad} is proposed in Fig. 7. $CH_3CH_2OH_{ad}$ (i.e., weakly bound ethanol) can be directly converted to CH_3CHO_{ad} by hydrogen abstraction. $CH_3CH_2OH_{ad}$ also could undergo heterolytic dissociation of O–H to produce $CH_3CH_2O_{ad}$ species [26]. $CH_3CH_2OH_{ad}$/$CH_3CH_2O_{ad}$ may react with either •OH or h^+ to produce I_{tran1}, I_{tran2}, I_{tran3}, and I_{tran4}, which represent the transient intermediates. The lifetimes of these transient intermediates time could be too short and their concentrations too small to be detected by our IR spectrometer. The reaction steps involved with photogenerated electron (e^-) and hole (h^+) will be further discussed. In summary, low-coverage ethanol (i.e., $CH_3CH_2OH_{ad}$/$CH_3CH_2O_{ad}$) on the H_2O_{ad}-containing TiO_2 surface could proceed through three parallel pathways: (i) pathway A, without involving I_{trans1}/I_{trans2}/I_{tran3}, to produce adsorbed C_1-oxygenated species (i.e., $HCHO_{ad}$, $HCOOH_{ad}$, and $HCOO^-_{ad}$); (ii) pathway B, to produce adsorbed C_2-oxygenated species (i.e., CH_3COOH_{ad} and $CH_3COO^-_{ad}$) and then C_1-oxygenated species; and (iii) pathway C, to produce CH_3CHO_{ad}, as shown in Fig. 7.

Figs. 5 and 6 also show that half-life for the adsorbed species to decrease their IR intensities to 50% of maximum value increased in the order $HCOOH_{ad} < HCOO^-_{ad} < CH_3COO^-_{ad} < CH_3CHO_{ad}$. The large half-life for the adsorbed species suggests its low reactivity for the reaction. CH_3CHO_{ad} exhibits the lowest reactivity, a manifestation of its slow rate of conversion to other intermediate species. The low reactivity of CH_3CHO_{ad} can also be inferred from its long decay time compared with that of ethanol, CH_3COOH_{ad}, and $HCHO_{ad}$ in previous PCO studies [22].

The effect of ethanol coverage on the reaction can be revealed by comparing Figs. 3 and 8, Figs. 4 and 9, Figs. 5 and 10, and Figs. 6 and 11. Upon UV illumination, the low-coverage ethanol reaction produced a prominent $HCOO^-_{ad}$ band at 1581 cm^{-1} (Fig. 3), whereas the high-coverage ethanol reaction generated a conspicuous $CH_3COO^-_{ad}$ band at 1438 cm^{-1} (Fig. 8). After the first 2 min of the reaction, the IR intensity of

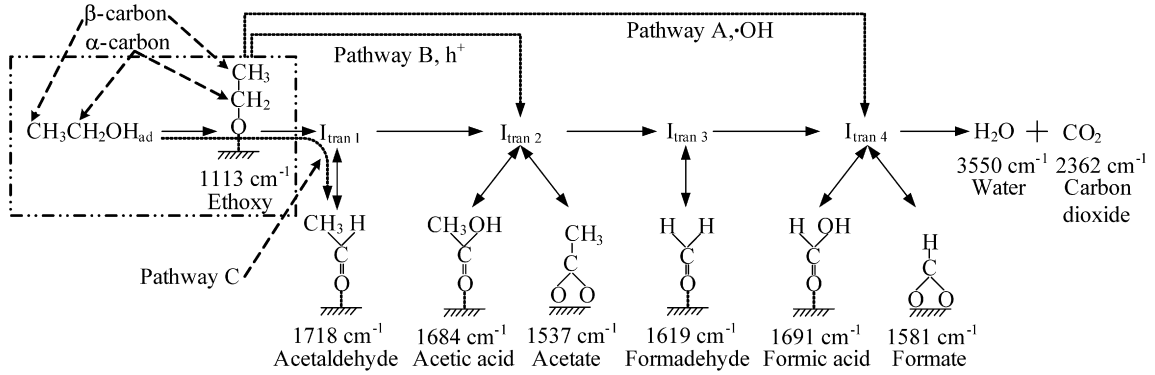

Fig. 7. Pathways for photocatalytic oxidation of ethanol.

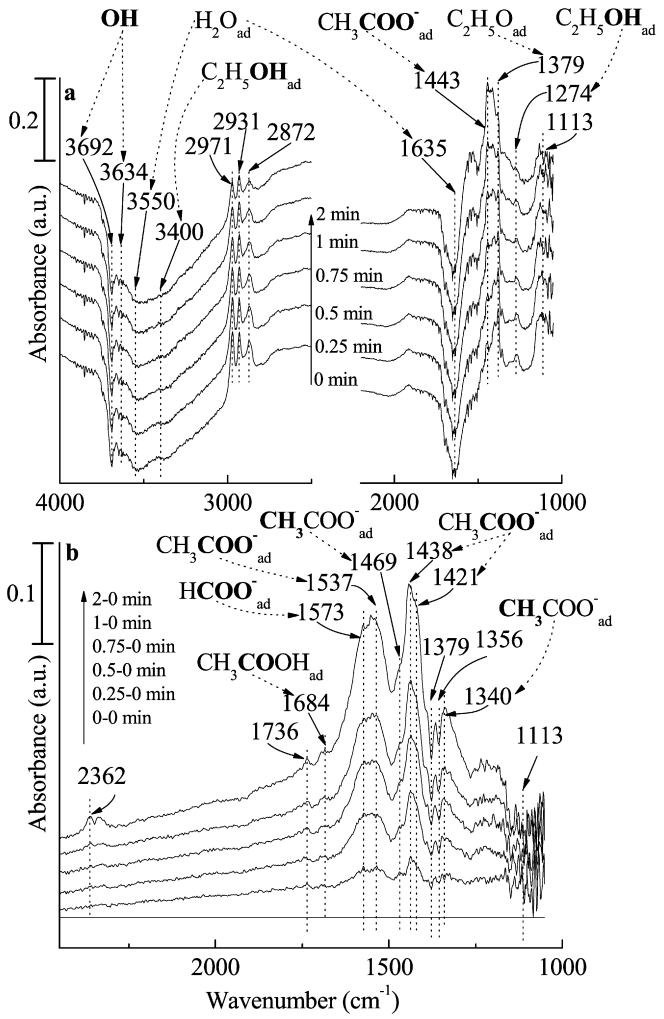

Fig. 8. (a) IR spectra and (b) difference spectra during the first 2 min of photocatalytic oxidation of high coverage ethanol.

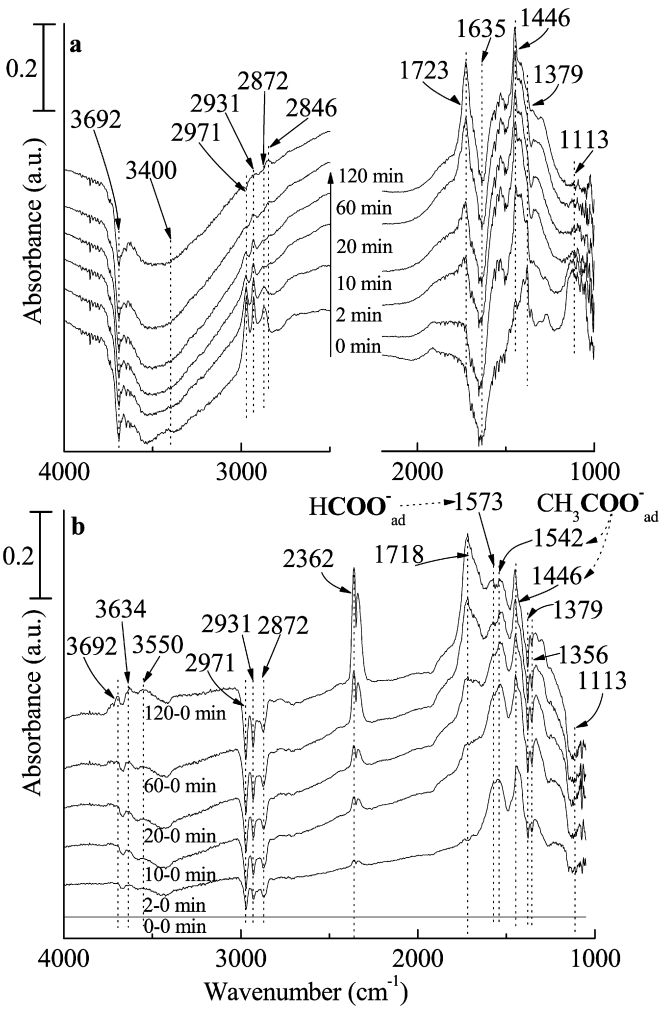

Fig. 9. (a) IR spectra and (b) difference spectra during 120 min of photocatalytic oxidation of high coverage ethanol.

$CH_3COO^-_{ad}$ in Fig. 8 was more than twice of that of $HCOO^-_{ad}$ in Fig. 3. The IR intensity ratio of $HCOO^-_{ad}$ to $CH_3COO^-_{ad}$ corresponded to the initial molar ratio of ethanol used for the low-coverage and high-coverage reactions in Fig. 2. Fig. 8 also shows that the formation of $CH_3COO^-_{ad}$ led that of other oxygenated species, indicating that most of the $CH_3COO^-_{ad}$ was produced from pathway B in Fig. 7. In contrast to the prominent $CH_3COO^-_{ad}$ band, the very weak CH_3CHO_{ad} band at 1736 cm^{-1} in Fig. 8b suggests that pathway C for the conversion of $CH_3CH_2OH_{ad}$/$CH_3CH_2O_{ad}$ to CH_3CHO_{ad} did not occur to a significant extent during the first 2 min of the reaction.

Gradual decay of the C–H bonds in $CH_3CH_2OH_{ad}$/$CH_3CH_2O_{ad}$ in Fig. 8a was accompanied by a growing $CH_3COO^-_{ad}$ band and a shoulder $HCOO^-_{ad}$ band with an increasing IR background in Fig. 8b. The increasing IR background was associated with the production of photogenerated electrons and is further discussed later. IR intensity profiles of the key species in Fig. 10 show that $CH_3CH_2OH_{ad}$ decayed at a higher rate than $CH_3CH_2O_{ad}$ and that significant CO_2 formation occurred only after 0.75 min of the reaction. It was also observed that the disappearance rate of $CH_3CH_2OH_{ad}$ was higher than that of $CH_3CH_2O_{ad}$ in the low-coverage ethanol reaction in Fig. 5.

As the high-coverage ethanol reaction proceeded beyond 2 min, the decline in the C–H stretching intensity of $CH_3CH_2OH_{ad}$ and $CH_3CH_2O_{ad}$ was accompanied by the increasing CH_3CHO_{ad}, CO_2, and H_2O_{ad} bands, shown in Fig. 9b. The IR intensities of $CH_3COO^-_{ad}$ and $HCOO^-_{ad}$ bands reached a maximum value at 20 min; the IR background intensity at 2000 cm^{-1} reached a maximum value at 30 min (Fig. 11). The rate of CO_2 formation further accelerated at 60 min, whereas the intensity of the IR background at 2000 cm^{-1} showed a substantial decrease, suggesting the photogenerated electrons may begin extensive participation in the oxidation of intermediate species to CO_2 and H_2O_{ad}.

4. Discussion

The coverage of $CH_3CH_2OH_{ad}$/$CH_3CH_2O_{ad}$ and H_2O_{ad} on the TiO_2 surface has a profound effect on how the photocatalytic oxidation is initiated. The key species that initiate the photocatalytic oxidation have been identified as •OH and h^+

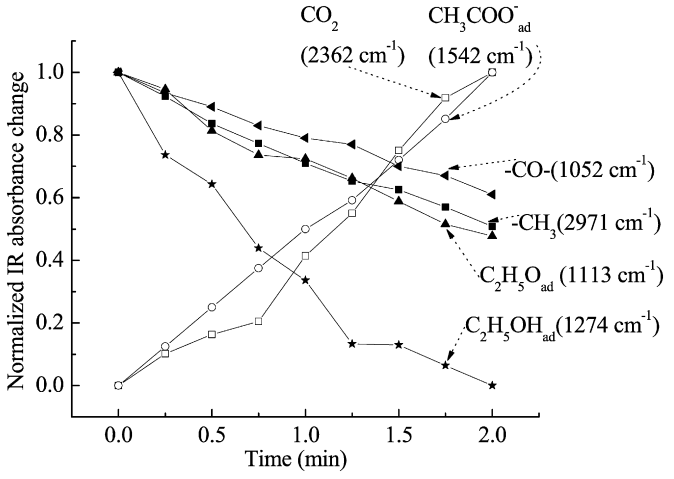

Fig. 10. Variation of the normalized IR intensity of adsorbed species and CO_2 as a function of time during the first 2 min of the photocatalytic oxidation of high coverage ethanol. Normalized intensity $= I(t)/I_{max}$, where $I(t)$: intensity of a species at time of t; I_{max}: the maximum intensity of a species during the first 2 min.

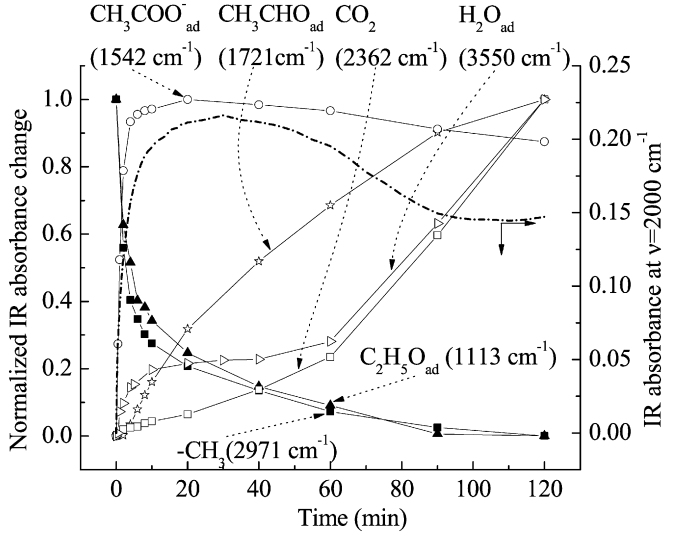

Fig. 11. Variation of the normalized IR intensity of adsorbed species and CO_2 as a function of time during 120 min of the photocatalytic oxidation of high coverage ethanol. Normalized intensity $= I(t)/I_{max}$, where $I(t)$: intensity of a species at time of t; I_{max}: the maximum intensity of a species during the 120 min.

[3,27–34]. The steps leading to the generation of these oxidizing species include:

$$TiO_2 + h\nu \rightarrow h^+ + e^-, \quad (1)$$

$$H_2O_{ad} \rightarrow OH^- + H^+, \quad (2)$$

$$OH^- + h^+ \rightarrow \bullet OH, \quad (3)$$

$$O_{2ad} + e^- \rightarrow O_2^-, \quad (4)$$

$$2O_2^- + 2H_2O_{ad} \rightarrow 2\bullet OH + 2OH^- + O_2. \quad (5)$$

Holes produced from UV illumination can react with H_2O_{ad} to produce •OH, whereas electrons must react through two key steps: (i) transfer of electrons from the TiO_2 surface to adsorbed oxygen (O_{2ad}) [i.e., step (4)] and (ii) the reaction of O_2^- with H_2O_{ad} to produce •OH [i.e., step (5)]. The simultaneous occurrence of all of these steps is required to avoid charge accumulation, which can retard the rates of the subsequent reaction steps in the photocatalytic oxidation.

The presence of H_2O_{ad} on the TiO_2 surface during the low-coverage ethanol reaction suggests that •OH would be available for initiating the reaction to proceed via pathway A in Fig. 7. It has been demonstrated that •OH can desorb from the TiO_2 surface, oxidizing the species that is not directly adsorbed on the TiO_2 surface [31,32]. Therefore, •OH could attack hydrogen on both α- and β-carbon in $CH_3CH_2OH_{ad}/CH_3CH_2O_{ad}$ and CH_3CHO_{ad}, as shown in Fig. 7. $CH_3CH_2OH_{ad}$ may adsorb in the form of multilayers through hydrogen bonding, as evidenced by a broad hump at 3400 cm^{-1}—a characteristic band of hydrogen bond in liquid ethanol [18]. The abstraction of hydrogen from β-carbon by •OH could lead to breaking of C–C bond, resulting in the formation of CHO_{ad} and $HCOO^-_{ad}$ [3,23, 24,35]. In contrast, the abstraction of hydrogen from α-carbon would lead to the formation of CH_3CHO_{ad} and CH_3COOH_{ad}. It should be noted that steps (6) and (7), which are not written as elementary steps, include only the initial reactants and key intermediates. The subsequent reactions for the conversion of $HCOO^-_{ad}/HCHO_{ad}/CH_3COO^-_{ad}/CH_3COO^-_{ad}$ to CO_2 and H_2O_{ad} have been reported [13,36–38]:

$$\begin{aligned} &CH_3CH_2OH_{ad}/CH_3CH_2O_{ad} + \bullet OH \\ &\quad \rightarrow \bullet CH_2CH_2OH_{ad}/\bullet CH_2CH_2O_{ad} + H_2O_{ad}, \\ &\qquad\qquad \downarrow O_{(lattice)}, O_2, \bullet OH \\ &\qquad CH_2O_{ad}/HCOO^-_{ad}/HCOOH_{ad}, \end{aligned} \quad (6)$$

$$CH_3CH_2OH_{ad} + 2\bullet OH \rightarrow CH_3CHO_{ad} + 2H_2O_{ad}. \quad (7)$$

The reactivity of α-carbon in ethanol with oxidizing species in homogeneous gas phase has been shown to decrease in the order •OH > O > O_2 [39]. The use of high O_2 concentration in this study could compensate for its low reactivity with ethanol radical, opening up a viable pathway for producing acid species.

The observation of $HCOOH_{ad}/HCOO^-_{ad}$ as primary intermediates suggests that the pathway A in Fig. 7 for the low-coverage ethanol reaction is mainly initiated by abstraction of hydrogen on the β-carbon via •OH. This reaction leads to the formation of $\bullet CH_2CH_2OH$, which can undergo C–C bond scission. The bond energy of C–C in alcohol and its radicals, such as ethanol (CH_3CH_2OH)/ethanol radical ($\bullet CH_2CH_2OH$), is about 15–20 kcal/mol lower than its C–H and O–H bonds [40,41]. In a homogeneous gaseous reaction, low bond energy reflects low activation energy for the bond scission reaction [40,41]. The activation energy for the C–C bond scission of an alcohol radical has been determined to be in the range of 13 kcal/mol [41], which is significantly lower than those of most heterogeneously catalytic reactions [42].

The presence of H_2O_{ad} with the low coverage of $CH_3CH_2OH_{ad}$ and CH_3CHO_{ad} has been shown to facilitate the replenishment of the lattice oxygen involved in oxidation [36]. Due to its high mobility, •OH produced from H_2O_{ad} can further oxidize CH_3CHO_{ad}, $CH_3COO^-_{ad}$, and $HCOO^-_{ad}$ species if its generation site is not blocked.

It has been well established that high-coverage ethanol displaced the majority of H_2O_{ad} from the TiO_2 surface [43]. The

lack of H_2O_{ad} would allow holes produced from UV illumination to react directly with $CH_3CH_2OH_{ad}/CH_3CH_2O_{ad}$ in the high-coverage ethanol reaction. Because holes cannot diffuse away from the TiO_2 surface, it is very likely that holes would abstract hydrogen from α-carbon, which is closer to the TiO_2 surface than β-carbon in $CH_3CH_2OH_{ad}$ and $CH_3CH_2O_{ad}$. The hydrogen abstraction process would initiate the pathway B in Fig. 7, producing $CH_3COO^-_{ad}$ species as a primary intermediate for the high-coverage ethanol reaction:

$$CH_3CH_2O_{ad} + h^+ + O_{(lattice)} \rightarrow CH_3COO^- + 2H^+, \quad (8)$$

$$CH_3CH_2OH_{ad} + 2h^+ + O_{(lattice)} \rightarrow CH_3COOH + 2H^+. \quad (9)$$

Consumption of holes by the foregoing reactions [44,45] would lead to the accumulation of photogenerated electrons if adsorbed oxygen and H_2O_{ad} were not available for removal of the electrons by steps (4) and (5). In Figs. 8, 9, and 11, the increasing IR intensity at 2000 cm^{-1}, a measure of accumulated electrons in or close to the conduction band [7–11], reflects the unavailability of oxygen and H_2O_{ad} on the TiO_2 surface during the initial high-coverage ethanol reaction. Thus, the hole-initiating oxidation of $CH_3CH_2OH_{ad}/CH_3CH_2O_{ad}$ could produce mainly $CH_3COO^-_{ad}$ species, leading to the buildup of the photogenerated electrons in or close to the conduction band of the TiO_2 catalyst. These hole-initiating and photogenerated electron buildup processes are further supported by Fig. 11, which shows the $CH_3COO^-_{ad}$ profile overlapped with that of the 2000 cm^{-1} intensity.

Due to the absence of mobile •OH and the inability of h^+ to diffuse away from the TiO_2 surface, only those species adsorbed on the h^+ generation sites can be oxidized. This could be one reason why adsorbed species produced from hole-initiating oxidation of the $CH_3CH_2OH_{ad}/CH_3CH_2O_{ad}$, accumulated on the TiO_2 surface and slowly converted to CO_2 and H_2O_{ad}. Hole-initiating oxidation appeared to dominate the high-coverage ethanol reaction until a significant amount of H_2O_{ad} accumulated on the TiO_2 surface. As H_2O_{ad} accumulated up to the level shown in the spectrum (60–0 min) in Fig. 9b, the adsorption of O_2 and transfer of electrons to adsorbed oxygen could occur to alleviate electron accumulation and produce •OH. These reaction steps shift the hole-initiating oxidation to the •OH-initiating oxidation, resulting in a parallel increase in CO_2 and H_2O_{ad} formation after 60 min of reaction, shown in Fig. 11.

Although the presence of H_2O_{ad} can facilitate the transfer of electron to adsorbed O_2, high coverage of H_2O_{ad} could lead to site blockage, inhibiting O_2 adsorption, slowing down and then terminating the electron-scavenging reaction [i.e., step (4)] [46]. The termination of this electron-scavenging reaction step appears to occur after 90 min of the reaction, at which time the IR intensity profile at 2000 cm^{-1}—a measure of the accumulation of photogenerated electrons—levels off while both H_2O_{ad} and acetaldehyde continue to grow in intensity.

Photocatalytic oxidation is generally considered a slow process, with an initial turnover frequency (TOF) in the range of 10^{-4}–10^{-5} s^{-1} [47,48] compared with the 10^{-2}–10^{-3} s^{-1} TOF of conventional heterogeneous catalysis [49–53]. In this study, the initial TOFs for CO_2 formation were determined to be 1.6×10^{-3} s^{-1} for the low-coverage reaction and 8.0×10^{-4} s^{-1} for the high-coverage reaction, assuming that each $CH_3CH_2OH_{ad}/CH_3CH_2O_{ad}$ molecule in first ethanol monolayer on the TiO_2 surface adsorbs on a single photocatalytic site. These TOFs for the CO_2 formation rate are significantly lower than those for C–H breaking (1.16×10^{-1} s^{-1} for the low-coverage reaction and 4.8×10^{-2} s^{-1} for the high-coverage reaction), indicating that the conversion of intermediate species such as CH_3CHO_{ad}, $HCOO^-_{ad}$, and $CH_3COO^-_{ad}$ to CO_2 and H_2O_{ad} is the rate-determining step for the photocatalytic oxidation of ethanol.

5. Conclusion

The reaction pathway for the photocatalytic oxidation of ethanol is strongly dependent on the coverage of $CH_3CH_2OH_{ad}/CH_3CH_2O_{ad}$ and H_2O_{ad}. In situ IR studies showed that the low-coverage ethanol reaction on the H_2O_{ad}-containing TiO_2 surface produced CO_2 and H_2O_{ad} via a parallel/series reaction pathway with $HCOO^-_{ad}$ as a major intermediate. The observed reaction products and their formation rates are consistent with a proposed •OH-initiating oxidation mechanism.

The high-coverage ethanol reaction on the H_2O_{ad}-deficient TiO_2 surface produced $CH_3COO^-_{ad}$ as a primary intermediate species, which can be further converted to CO_2 and H_2O_{ad} through $HCHO_{ad}/HCOOH_{ad}/HCOO^-_{ad}$. The absence of H_2O_{ad} participation in the initial ethanol oxidation suggests that the high-coverage ethanol reaction is initiated by holes which abstract hydrogen from α-carbon of $CH_3CH_2OH_{ad}/CH_3CH_2O_{ad}$ to produce $CH_3COO^-_{ad}/CH_3COOH_{ad}$. The participation of holes in oxidation and the absence of adsorbed oxygen for interacting with photogenerated electrons results in an accumulation of photogenerated electrons, thereby increasing the IR background spectrum. As the reaction proceeded, a buildup of the final product H_2O_{ad} and decreased $CH_3CH_2OH_{ad}/CH_3CH_2O_{ad}$ coverage allowed adsorption of O_2 onto the TiO_2 surface, leading to •OH formation and an accelerated rate of CO_2/H_2O_{ad} formation. Despite of a high oxidation potential of hole, •OH is more effective than hole for the oxidation of $CH_3CH_2OH_{ad}$ and $CH_3CH_2O_{ad}$ to CO_2 and H_2O_{ad}.

Acknowledgments

This work was partially supported by the Ohio Board of Regents (Grant R4552-OBR) and the US Department of Energy (Grant DE-FG26-01NT41294).

References

[1] P.V. Kamat, Chem. Rev. 93 (1993) 267.
[2] M.A. Fox, M.T. Dulay, Chem. Rev. 93 (1993) 341.
[3] M.R. Hoffmann, S.T. Martin, W. Choi, D.W. Bahnemann, Chem. Rev. 95 (1995) 69.
[4] A.L. Linsebigler, G. Lu, J.T. Yates Jr., Chem. Rev. 95 (1995) 735.
[5] A. Mills, S. Le Hunte, J. Photochem. Photobiol. A 108 (1997) 1.
[6] D.F. Ollis, Cattech 2 (1998) 149.
[7] A. Yamakata, T.-A. Ishibashi, H. Onishi, J. Mol. Catal. A Chem. 199 (2003) 85.

[8] S.H. Szczepankiewicz, A.J. Colussi, M.R. Hoffmann, J. Phys. Chem. B 104 (2000) 9842.
[9] S.H. Szczepankiewicz, J.A. Moss, M.R. Hoffmann, J. Phys. Chem. B 106 (2002) 7654.
[10] D.A. Panayotov, J.T. Yates Jr., Chem. Phys. Lett. 410 (2005) 11.
[11] T. Berger, M. Sterrer, O. Diwald, E. Knoezinger, D. Panayotov, T.L. Thompson, J.T. Yates Jr., J. Phys. Chem. B 109 (2005) 6061.
[12] W.-C. Wu, C.-C. Chuang, J.-L. Lin, J. Phys. Chem. B 104 (2000) 8719.
[13] L.-F. Liao, W.-C. Wu, C.-Y. Chen, J.-L. Lin, J. Phys. Chem. B 105 (2001) 7678.
[14] J.M. Coronado, S. Kataoka, I. Tejedor-Tejedor, M.A. Anderson, J. Catal. 219 (2003) 219.
[15] M. El-Maazawi, A.N. Finken, A.B. Nair, V.H. Grassian, J. Catal. 191 (2000) 138.
[16] http://Webbook.Nist.Gov/Chemistry/, accessed on September 1, 2006.
[17] J. Arana, C.G.I. Cabo, J.M. Dona-Rodriguez, O. Gonzalez-Diaz, J.A. Herrera-Melian, J. Perez-Pena, Appl. Surf. Sci. 239 (2004) 60.
[18] N.B. Colthup, L.H. Daly, S.E. Wiberley, Introduction to Infrared and Raman Spectroscopy, third ed., Academic Press, Boston, 1990.
[19] W. Rachmady, M.A. Vannice, J. Catal. 207 (2002) 317.
[20] J. Rasko, T. Kecskes, J. Kiss, Appl. Catal. A 287 (2005) 244.
[21] O. Levenspiel, Chemical Reaction Engineering, third ed., Wiley, New York, 1999.
[22] M.R. Nimlos, E.J. Wolfrum, M.L. Brewer, J.A. Fennell, G. Bintner, Environ. Sci. Technol. 30 (1996) 3102.
[23] D.S. Muggli, J.T. Mccue, J.L. Falconer, J. Catal. 173 (1998) 470.
[24] D.S. Muggli, K.H. Lowery, J.L. Falconer, J. Catal. 180 (1998) 111.
[25] J.C. Kennedy, A.K. Datye, J. Catal. 179 (1998) 375.
[26] H. Idriss, E.G. Seebauer, J. Mol. Catal. A Chem. 152 (2000) 201.
[27] K. Ikeda, H. Sakai, R. Baba, K. Hashimoto, A. Fujishima, J. Phys. Chem. B 101 (1997) 2617.
[28] R. Gao, J. Stark, D.W. Bahnemann, J. Rabani, J. Photochem. Photobiol. A 148 (2002) 387.
[29] D.-R. Park, J. Zhang, K. Ikeue, H. Yamashita, M. Anpo, J. Catal. 185 (1999) 114.
[30] O.M. Alfano, M.I. Cabrera, A.E. Cassano, J. Catal. 172 (1997) 370.
[31] M.C. Lee, W. Choi, J. Phys. Chem. B 106 (2002) 11818.
[32] Y. Murakami, E. Kenji, A.Y. Nosaka, Y. Nosaka, J. Phys. Chem. B 110 (2006) 16808.
[33] M.M. Ameen, G.B. Raupp, J. Catal. 184 (1999) 112.
[34] Y. Du, J. Rabani, J. Phys. Chem. B 107 (2003) 11970.
[35] M.C. Blount, J.A. Buchholz, J.L. Falconer, J. Catal. 197 (2001) 303.
[36] D.S. Muggli, J.L. Falconer, J. Catal. 181 (1999) 155.
[37] M.J. Backes, A.C. Lukaski, D.S. Muggli, Appl. Catal. B 61 (2005) 21.
[38] D.S. Muggli, M.J. Backes, J. Catal. 209 (2002) 105.
[39] N. Washida, J. Chem. Phys. 75 (1981) 2715.
[40] H. Sun, J.W. Bozzelli, J. Phys. Chem. A 105 (2001) 9543.
[41] H. Sun, J.W. Bozzelli, J. Phys. Chem. A 106 (2002) 3947.
[42] C.N. Satterfield, Heterogeneous Catalysis in Industrial Practice, second ed., Krieger, Malabar, 1996.
[43] Y. Suda, T. Morimoto, M. Nagao, Langmuir 3 (1987) 99.
[44] D.C. Hurum, A.G. Agrios, K.A. Gray, T. Rajh, M.C. Thurnauer, J. Phys. Chem. B 107 (2003) 4545.
[45] A. Yamakata, T. Ishibashi, H. Onishi, J. Phys. Chem. B 106 (2002) 9122.
[46] M.A. Henderson, W.S. Epling, C.H.F. Peden, C.L. Perkins, J. Phys. Chem. B 107 (2003) 534.
[47] D.S. Muggli, S.A. Larson, J.L. Falconer, J. Phys. Chem. 100 (1996) 15886.
[48] B. Sun, P.G. Smirniotis, Catal. Today 88 (2003) 49.
[49] H.S. Fogler, Elements of Chemical Reaction Engineering, fourth ed., Prentice–Hall PTR, Upper Saddle River, 2005.
[50] M.A. Brundage, S.S.C. Chuang, J. Catal. 164 (1996) 94.
[51] M. Boudart, Chem. Rev. 95 (1995) 661.
[52] W. Zhang, A. Desikan, S.T. Oyama, J. Phys. Chem. B 99 (1995) 14468.
[53] S.L. Shannon, J.G. Goodwin Jr., Chem. Rev. 95 (1995) 677.